RF Electro-magnetic Field Effects on the 571.2MHz Normal Conducting Sub-harmonic Buncher

PEI Shi-Lun[1,2;1)] WANG Shu-Hong[1]

1 (Institute of High Energy Physics, CAS, Beijing 100049, China)
2 (Graduate School of Chinese Academy of Sciences, Beijing 100049, China)

Abstract Usually, the RF electro-magnetic field can affect the resonant cavity in two ways. One is the heat loading to the cavity due to the RF power dissipation, and another is the Lorenz force due to the high RF surface field. In this paper, the RF electro-magnetic field effects on the Sub-harmonic Buncher 2 (SHB2) are described and some results presented and discussed. The analyses of the RF electro-magnetic field effects were performed by coupled simulations with finite difference method software-Superfish and finite element method software–ANSYS. In addition, the RF electro-magnetic field effects on the Sub-harmonic Buncher 1 (SHB1) are also described.

Key words RF heating, Lorenz force, Superfish, ANSYS, frequency shift

1 Introduction

To have a new pre-injector with good bunching characteristics, BEPC Ⅱ's (the upgrade project of BEPC, Beijing Electron Positron Collider) future pre-injector has been designed and optimized by introducing two sub-harmonic bunchers (SHBs)[1]. Both the two SHBs are reentrant cavities. In this new pre-injector, the SHB frequencies (142.8MHz for SHB1, 571.2MHz for SHB2) as well as the linac frequency (2856MHz) need to be phase-locked to the ring frequency (499.8MHz) rigorously to ensure precise injection timing and make the injection flexible, so the frequency stability of the 2 SHBs becomes important.

In order to increase the frequency stability of the two SHBs, the RF electro-magnetic field effects on the SHBs need to be evaluated and cured. In this paper, the RF electro-magnetic field effects on SHB2 are described and some results presented and discussed. Since the operating frequency is lower than 1000MHz, the skin depth is larger than 2.5μm. The maximum accelerating gradient is smaller than 4.0MV/m. With the RF filling pulse of 50μs and the repetition rate of 50Hz, the total pulsed power dissipation will be 7kW. Here we only concentrate on the average effects of the RF electro-magnetic fields instead of the transient effects[2]. The transient effects are usually concentrated in the superconducting structures due to their particularities. The analyses of the RF electro-magnetic field effects were performed by coupled simulations with finite difference method software–Superfish[3] and finite element method software–ANSYS[4]. Using the same analytical method, the RF electro-magnetic field effects on SHB1 are also described. In addition, the optimized cure method of the RF heating effect is proposed for the two SHBs.

2 Basic theory

Usually, the RF electro-magnetic field can affect the resonant cavity in two ways. One is the heat loading to the cavity due to the RF power dissipation, and another is the Lorenz force due to the high RF sur-

Received 5 January 2005, Revised 9 March 2005
1) E-mail: peisl@mail.ihep.ac.cn

face field. Both of them can distort the structure of the resonant cavity. The former can be mitigated by correct water cooling, and the latter can be eased by appropriately choosing material and cavity stiffening.

The SHB2 is an axial symmetrical reentrant cavity, so 2D analysis of the RF electro-magnetic field effects on the cavity could be enough. In our analyses, Superfish is used to calculate the RF electro-magnetic fields, and ANSYS is used to calculate the RF heating effect and the Lorenz force effect caused by the RF electro-magnetic fields. Although ANSYS can also be used to calculate the RF electro-magnetic fields, Superfish is more professional.

Since Superfish and ANSYS use different meshes, some data exchange from Superfish output to ANSYS input need to be made. After the electro-magnetic output data are scaled to the real cavity power loss with $P \propto E^2 \propto H^2$, the power loss density P_s caused by surface resistance and the Lorenz force density F_s caused by surface charge and surface current on each mesh point of the cavity inner surface are[5, 6]

$$P_s = \frac{1}{2} R_s H_s^2 = \frac{1}{2} \frac{H_s^2}{\sigma\delta} = \frac{1}{2} H_s^2 \sqrt{\pi f \mu_0 / \sigma}$$

and

$$F_s = \frac{1}{4}(\mu_0 H_s^2 - \varepsilon_0 E_s^2) \quad ,$$

where R_s is the surface resistance, H_s the surface magnetic field, σ the conductivity, δ the skin depth, f the resonate frequency, μ_0 the space permeability, E_s the surface electric field, and ε_0 the space permittivity.

The power loss density and the Lorenz force density can be used as the heat flux and pressure loads, respectively, in ANSYS. To let the temperature distribution reach a stable state in the RF heating effect analyses, water cooling is necessary, so the convection coefficient of the water cooling tubes should be calculated by some empirical formulas[7] which are different in different situations. In ANSYS, the convection coefficient loads can be used to simulate a forced convection boundary condition.

The structure distortions caused by the RF heating effect and the Lorenz effect result in the frequency shift of the cavity, which can be calculated by the Slater perturbation method[8]. The frequency shift $\mathrm{d}f$ is a function of the volume $\mathrm{d}V$ located on the inner cavity surface, as well as the surface magnetic field H_s and the surface electric field E_s, which is given by

$$\frac{\mathrm{d}f}{f} = \frac{\int_{\Delta V}(\mu_0 H_s^2 - \varepsilon_0 E_s^2)\mathrm{d}V}{4U} = \frac{\int_{\Delta V}(\mu_0 H_s^2 - \varepsilon_0 E_s^2)\mathrm{d}V}{\int_V (\mu_0 H^2 + \varepsilon_0 E^2)\mathrm{d}V} \quad .$$

Here H and E are the magnetic field and the electric field in the inner part of the cavity, respectively. They are different from H_s and E_s.

3　RF electro-magnetic fields analyses

To get better RF characteristics, the structure and geometric parameters of the SHB2 cavity have been studied and optimized[9] with the software Superfish, as shown in Fig. 1. The electro-magnetic field's distribution in the SHB2 cavity is shown in Fig. 2. In order to improve the water cooling capability and reduce the frequency shift caused by the gap distance change when the input power increases, copper was selected to be the structural material with the properties listed in Table 1.

Table 1.　Material properties of copper[4].

Possion's ratio	0.3
density/(kg/m^3)	8.9×10^3
elastic modulus/Pa	1.172×10^{11}
thermal conductivity/(W/m/K)	393
thermal expansion coefficient/(μm/m/K)	1.656×10^{-5}

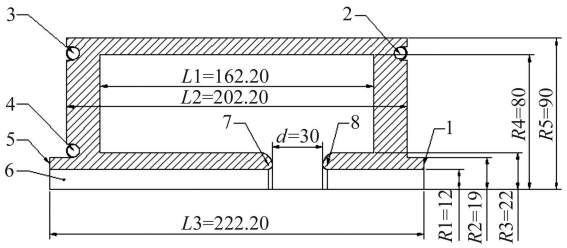

Fig. 1. Schematic diagram of SHB2 cavity (unit: mm).
1. short drift end; 2. water cooling tube 1; 3. water cooling tube 2; 4. water cooling tube 3; 5. long drift end; 6. beam hole; 7. long drift nose; 8. short drift nose.

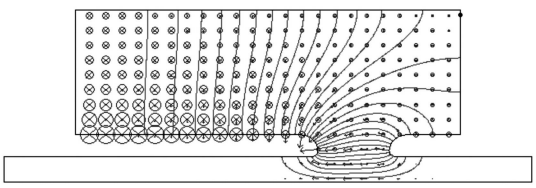

Fig. 2. RF electro-magnetic fields distribution in the SHB2 cavity.

4 RF heating effect analysis

In the SHB2 cavity, three water cooling tubes with an inner diameter d_1 of 7.3mm and an outer diameter d_2 of 8.0mm are used. The distance R between their center and the cavity axis is 81mm for water cooling tube 1 and 2, and 23mm for water cooling tube 3. The cooling water flow velocity w and temperature T are assumed to be 1.5m/s and 45°C, respectively. With the cooling water properties shown in Table 2, the Reynolds number Re is

$$Re = \frac{wd_1}{v} = \frac{1.5\text{m/s} \times 7.3 \times 10^{-3}\text{m}}{6.075 \times 10^{-7}\text{m}^2/\text{s}} = 18024.7 \ .$$

Since $120000 > Re > 10000$ and $120 > Pr > 0.7$, the convection coefficient α for the three water cooling tubes can be obtained by the following empirical formula[7]

$$\alpha = 0.023 Re^{0.8} Pr^{0.4} \varepsilon_1 \frac{\lambda}{d_1} \left[1 + 10.3 \left(\frac{d_1}{R}\right)^3\right] \ ,$$

where ε_1 is a modifying factor for the water cooling tube length $L = 2\pi R$. For water cooling tubes 1 and 2, ε_1 is 1, and for water cooling tube 3, ε_1 is 1.09. Hence the convection coefficients for the three water cooling tubes are 8945W/m^2/K, 8945W/m^2/K and 12778W/m^2/K, respectively.

Table 2. Physical properties of the cooling water[7].

Prandtl number Pr	3.925
viscous damping coefficient ν/(m^2/s)	6.075×10^{-7}
heat transfer coefficient λ/(W/m/K)	0.6415

In ANSYS, after the cavity material has been set and the PLANE55 mesh created, the heat flux and the convection coefficient loads can be applied. Then, the temperature distribution on the cavity wall can be calculated. Fig. 3 shows one typical calculation result for $P_{\text{average}} = 7\text{kW} \times 50\mu\text{s} \times 50\text{Hz}$=17.5W with the water cooling tube 1 and 2 used, indicating that the largest power loss density is usually located near the long drift end and the highest temperature at the long drift nose.

After obtaining the temperature distribution result, we can transform the PLANE55 mesh to the PLANE42 mesh. Then the structure distortion can be calculated by applying the thermal distribution results as loads. In addition, correct displacement constraints need to be defined as realistically as possible, since the constraints may dominate the structure distortion. Once the structure distortion has been obtained, APDL (ANSYS Parametric Design Language) script language[4] can be used to calculate the frequency shift by the Slater perturbation method.

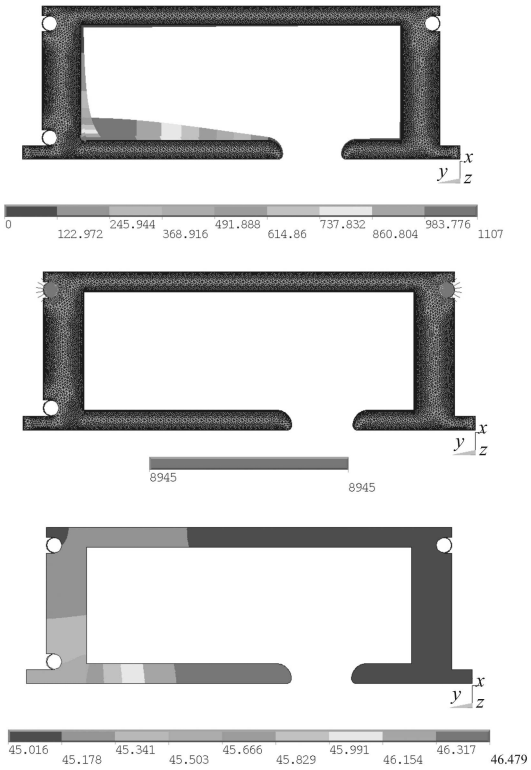

Fig. 3. The heat flux loads applied (upper) (unit: W/m^2); the convection coefficient loads applied (middle) (unit: W/m^2/K); the resulting temperature distribution (lower) (unit: ℃).

In the RF heating effect analysis, seven different water cooling schemes have been studied: a) water cooling tube 1 is used; b) water cooling tube 2 is used; c) water cooling tube 3 is used; d) water cooling tubes 1 and 2 are used; e) water cooling tubes 1 and 3 are used; f) water cooling tubes 2 and 3 are used; g) water cooling tubes 1, 2 and 3 are used. For each cooling scheme, three kinds of fixation schemes have been considered: a) short drift end is fixed in all DOF; b) long drift end is fixed in all DOF; c) both short and long drift ends are fixed in all DOF. Table 3 shows the calculation results for all kinds of cooling and fixation schemes.

Table 3. Calculation results for all kinds of cooling and fixation schemes.

cooling scheme	fixation scheme	Max. temperature/℃	Max. distortion/μm	Freq. shift/Hz
a	a	47.88	3.88	−18113.10
a	b	47.88	5.63	−18108.31
a	c	47.88	5.46	−22810.57
b	a	46.52	1.43	−8322.05
b	b	46.52	2.58	−8331.52
b	c	46.52	2.53	−10049.28
c	a	46.61	3.10	−12356.50
c	b	46.61	2.94	−12368.17
c	c	46.61	2.55	−16410.51
d	a	46.48	1.95	−7211.84
d	b	46.48	2.49	−7218.57
d	c	46.48	2.46	−8001.96
e	a	46.26	1.48	−8256.57
e	b	46.26	2.29	−8262.99
e	c	46.26	2.25	−9462.70
f	a	46.25	1.25	−6995.03
f	b	46.25	1.94	−6999.83
f	c	46.25	1.90	−8023.53
g	a	46.23	1.65	−6242.82
g	b	46.23	1.91	−6246.31
g	c	46.23	1.89	−6616.53

By comparing the results, one can get the following conclusions:

1) Obviously speaking, cooling scheme g) is the best one, which has the lowest temperature increase, the least distortion and the smallest frequency shift.

2) In all of the fixation schemes, fixation scheme a) is the best one, which has the least distortion and the smallest frequency shift. Scheme b) is a little worse than scheme a).

3) By choosing appropriate cooling scheme, not only can the temperature increase be decreased, the distortion and the frequency shift can also be lowered. By choosing appropriate fixation scheme, only the distortion and the frequency shift can be lowered.

4) As a whole, the cooling capability of water cooling tube 2 is greater than that of water cooling tube 3, and water cooling tube 3 is greater than tube 1.

5) In each scheme, the temperature increase is not very high, and the maximum distortion is smaller than the mechanical tolerance of 5μm.

6) For any cooling scheme, the ratio of the frequency shift to the 2MHz tuning range is smaller than 1%, which can be neglected. However, it is impossible to keep the frequency stable without any water cooling.

7) From the view point of fabrication, due to the small distance between water cooling tube 3 and the beam tube, some compromises must be made. Using the water cooling tubes of 1 and 2 might be more realistic.

Fig. 4 shows the distortion distribution results corresponding to the cooling scheme d) and the three different fixation schemes, indicating that the maximum distortion is usually located at the long drift nose.

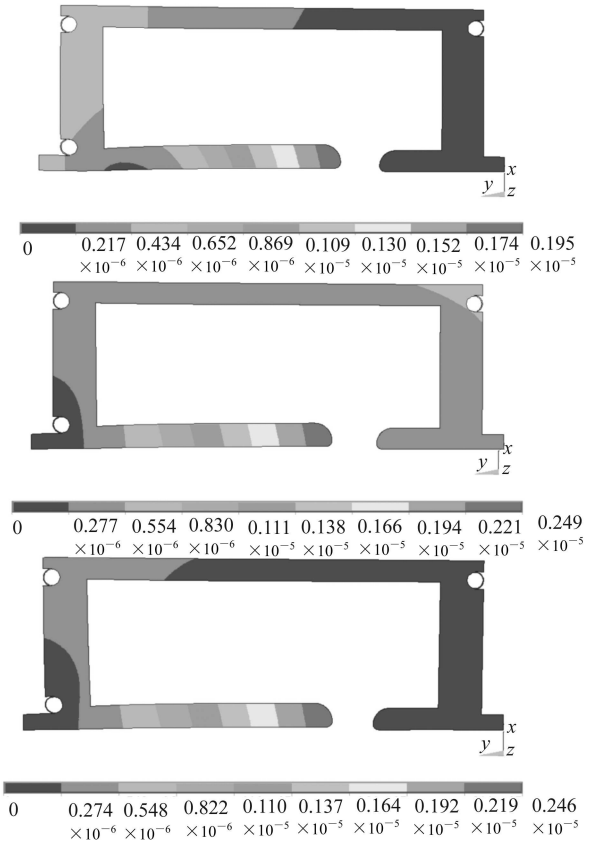

Fig. 4. Distortion distribution results corresponding to the cooling scheme d) and the three different fixation schemes (unit: m).

5 Lorenz force effect analysis

In the Lorenz force effect analysis, after the PLANE42 mesh has been created, the APDL script language can be used to calculate the Lorenz force density and the corresponding frequency shift. Fig. 5 shows the Lorenz force distribution in the cavity and the resulting distortion distribution with fixation scheme c). At the short drift nose and the long

drift nose, because the stored electric energy is higher than the stored magnetic energy, Lorenz force points inward, this decreases the effective cavity volume. While near the long drift end, the Lorenz force and the cavity volume perform the opposite behavior. By the Slater perturbation method, we know that this decreases the cavity frequency.

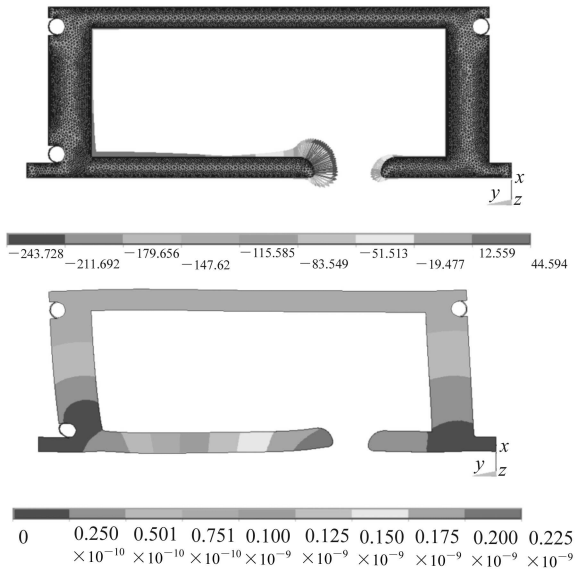

Fig. 5. The Lorenz distribution (upper with unit: N/m^2) and the distortion distribution in the cavity (lower with unit: m).

Table 4 shows the maximum distortion and the corresponding frequency shift with three different fixation schemes when the input pulsed power is 7kW. The maximum distortion is less than 1nm, and the frequency shift is only several Hz. Fixation scheme c) is better than the other two schemes with the least distortion and the smallest frequency shift. However, compared with the RF heating effects, the Lorenz effect on the normal conducting RF cavities can be neglected.

Table 4. Calculation results for all kinds of fixation schemes.

fixation scheme	Max. distortion/nm	Freq. shift/Hz
a	0.753	−1.92
b	0.598	−1.94
c	0.225	−1.12

6 Analysis on the SHB1

Similar to the SHB2, the SHB1 is a 10kW/70μs /142.8MHz/50Hz copper reentrant cavity[10], both the average power dissipation and the cavity volume are larger than those of the SHB2. If the same cooling method and fixation method are adopted, then the maximum temperature might be very high, the ratio of the frequency shift to the 200kHz tuning range might be larger than 1%, and the maximum distortion might be larger than the mechanical tolerance of 5μm. Using the same analytical method, the RF heating effect on the SHB1 is also studied. Table 5 shows the calculation result of the RF heating effect on the SHB1 with the seven cooling schemes and fixation scheme c), indicating that the cooling schemes of the SHB2 are not very effective for the SHB1 because of the larger cavity volume.

Table 5. Calculation results for all kinds of cooling schemes.

cooling scheme	Max. temperature/℃	Max. distortion/μm	Freq. shift/Hz
a	60.96	125.00	−24088.97
b	51.49	44.00	−6962.24
c	51.69	45.00	−8228.68
d	51.43	43.90	−7297.94
e	51.47	43.90	−8424.61
f	50.95	39.40	−6627.83
g	50.93	39.50	−6920.71

In order to increase the frequency stability of the SHB1, the water cooling becomes even more important. Both the two end plates and the long drift tube need water cooling[11]. In the meantime, water cooling of the walls of the long drift tube should be simple. One idea is to insert an open-ended copper tube into 1–4 slightly larger diameter holes drilled into the long drift tube wall. The cooling water flows first through the copper tube, then back through the space between the copper tube and the hole in the drift tube wall. A spacer can be spiraled around the copper tube. Another idea is to make 4 long holes along the long drift tube for water cooling. Near the long drift nose, every two holes are connected with a cap, which is shielded by electron beam welding. From the view point of fabrication, the former method might be simpler.

7 Summary

Using Superfish and ANSYS, we study the RF electro-magnetic field effects on the normal conduc-

ting RF cavities, indicating that the main effect is the RF heating effect, and the Lorenz effect can be neglected. This is contrary to the superconducting structures, where the main effect is the Lorenz effect. In addition, the optimized cure method of the RF heating effect is proposed for the two SHBs of BEPCⅡ future pre-injector. With the same kind of cavity structure, the larger the cavity volume, the more complicated the cure method of the RF heating effect. The analyses of the RF electro-magnetic field effects are not only very helpful for choosing the water cooling scheme and the fixation scheme, but also very meaningful for choosing the resonate frequency's tuning range and the structure's mechanical tolerance. In a word, it provides much reference information for the cavity's RF design and structure design.

We thank Prof. S. Ohsawa from KEK and Prof. J. Clendenin from SLAC for their very helpful discussions and some good advices.

References

1 PEI Shi-Lun, WANG Shu-Hong, GU Peng-Da et al. High Energy Phys. and Nucl. Phys., 2004, **28**(5): 549 (in Chinese)
(裴士伦, 王书鸿, 顾鹏达等. 高能物理与核物理, 2004, **28**(5): 549)

2 Joshi S C, Paramonov V, Skassyrskaya A et al. The Complete 3-D Coupled RF-Thermal-Structural-RF Analysis Procedure for a Normal Conducting Accelerating Structure for High Intensity Hadron Linac. Proc. of LINAC 2002. Gyeongju, Korea. 216

3 Billen J H, Young L M . Possion Superfish: LA-UR-96-1834. Los Alamos National Laboratory, 2002

4 ANSYS Collaboration. Manual of Electromagnetic Field Analysis in ANSYS. America: ANSYS Inc., 2000

5 Hartman N, Rimmer R A. Electromagnetic, Thermal, and Structural Anasysis of RF Cavities Using ANSYS. Proc. of the 2001 Particle Accelerator Conference. Chicago, America

6 ZHOU Ke-Ding, ZHANG Su-Wen, DONG Tian-Lin et al. Electromagnetic Field Theory Fundamentals. Beijing: China Machine Press, 2000. 214 (in Chinese)
(周克定, 张肃文, 董天临等. 北京: 机械工业出版社, 2000. 214)

7 XU Zhao-Jun. Heat Transfer Theory. Beijing: China Machine Press, 1980. 57 (in Chinese)
(许肇钧. 北京: 机械工业出版社, 1980. 57)

8 David M. Pozar. Microwave Engineering(2nd Edition). New York: John Wiley & Sons, 1998. 341

9 PEI Shi-Lun, WANG Shu-Hong, GU Peng-Da. Atomic Energy Science and Technology, Accepted (in Chinese)
(裴士伦, 王书鸿, 顾鹏达. 原子能科学技术, 已接收)

10 PEI Shi-Lun, WANG Shu-Hong, GU Peng-da et al. High Power Laser and Particle Beams, 2004, **16**(6): 795 (in Chinese)
(裴士伦, 王书鸿, 顾鹏达等. 强激光与粒子束, 2004, **16**(6): 795)

11 PEI Shi-Lun. Some Topics of BEPCⅡ Linac: IHEP-AC-MW-Note/2004-02. Internal Report, IHEP, March, 2004

571.2MHz次谐波聚束腔的高频电磁场效应

裴士伦[1,2;1)]　王书鸿[1]

1 (中国科学院高能物理研究所　北京　100049)
2 (中国科学院研究生院　北京　100049)

摘要　高频谐振腔中的电磁场通常以两种方式影响谐振腔的特性. 一种方式是通过作用在谐振腔内壁上的高频热, 这主要由高频功率的欧姆损耗导致; 另一种方式是通过作用在谐振腔内壁上的洛仑兹力, 这主要由谐振腔内壁上的面电流和面电荷导致. 联合使用有限差分软件Superfish和有限元软件ANSYS，本文对571.2MHz次谐波聚束腔中的高频电磁场效应进行了研究. 此外, 本文还对BEPCⅡ未来预注入器第1个次谐波聚束腔中的高频热效应进行了讨论.

关键词　高频热　洛仑兹力　Superfish　ANSYS　频移

2005 – 01 – 05 收稿,　2005 – 03 – 09 收修改稿

1) E-mail: peisl@mail.ihep.ac.cn